SAND2021-12137C

Distortion Effects in CSP Mirror Reflections

Randy C. Brost

Sandia National Laboratories
P.O. Box 5800, MS 1127
Albuquerque, NM 87185-1127 USA

rcbrost@sandia.gov

Abstract. Concentrating solar power (CSP) mirrors must have high optical accuracy to achieve desired performance, which drives a need for accurate metrology systems. One approach to mirror metrology is to provide an optical target of known geometry and view its reflection to assess the location of known features. Such systems require reliable feature recognition to establish the correspondence between the target object and reflected image. Meanwhile, reflections in CSP mirrors exhibit distortion due to mirror curvature and slope errors. At small magnitudes, these distortions are beneficial because they provide an indication of mirror surface shape. However, excessive distortion magnitudes can confound metrology systems by making feature recognition and correspondence difficult. In this paper we explore the phenomenon of reflected image distortions both empirically and analytically. We show experimental data where the same object seen reflected in the same mirror can exhibit small to gross distortion, merely by varying the image capture parameters of target-to-mirror and camera-to-mirror distance. We present an analytic model explaining this phenomenon and show how it explains the observed results. We then extend the model to derive an equation for metrology system sensitivity.

INTRODUCTION

Concentrating solar power (CSP) systems employ high concentration ratios to achieve high temperatures for efficient energy production. This requires high optical precision, which can be especially challenging for central receiver systems, where heliostat-to-receiver distances may exceed 1.5 km. Validating, tuning, and monitoring heliostat optical performance requires metrology tools capable of precisely measuring heliostat mirrors in the outdoor environment.

One important class of CSP mirror metrology systems is based on the principle of finding features in reflected images and analyzing their observed location to determine local mirror slope. Figure 1 illustrates an example. Here a camera views the reflection of an optical target of known geometry, and analyzes the reflected image to infer mirror shape, both nominal slope and slope error. Several metrology systems based on this principle have been reported, including tower-based methods of measuring canting angles [1], and systems utilizing unmanned aircraft systems (UAS) for measuring heliostat canting angles [2], heliostat slope, canting, and pointing errors [3], and combined inspection/metrology systems [4]. All of these examples operate by viewing the reflection of known optical target features and measuring the displacement between observed reflected feature locations compared to the locations expected for an ideal optical system.

As illustrated in Figure 1, these reflections are distorted due mirror shape. These distortions can be beneficial, because they provide a signal indicating mirror surface slope. However, feature-based metrology systems all fundamentally rely on matching features in a reflected image against corresponding features of a real-world object; if distortion is too high, this correspondence may become difficult or impossible to resolve. Thus, excessive distortion can confound these systems.

In this paper we study the distortion effect, and investigate several key questions:

- What levels of distortion are seen with real CSP mirrors?
- How does it vary with image capture conditions?
- Why does it occur?
- How do we exploit it?

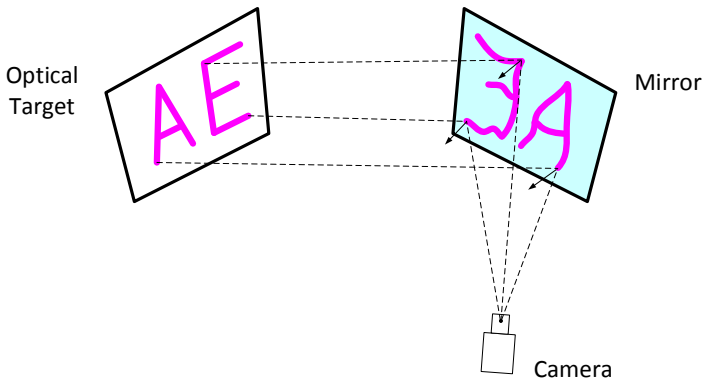

FIGURE 1. Feature-based mirror metrology.

As we shall see, distortion induced by real CSP mirrors can be extremely high depending on image capture conditions, but these conditions are readily characterized by a simple mathematical equation relating target-to-mirror distance, camera-to-mirror distance, and view incidence angle. The following sections will present a systematic empirical study observing the variation in distortion with image capture conditions, followed by a mathematical model of distortion effects as a function of these key parameters.

SYSTEMATIC DISTORTION OBSERVATIONS

As noted above, distortion in the reflection of an optical target can be beneficial because it provides an indication of mirror surface shape, but excessive distortion can cause metrology systems to fail because of the difficulty of identifying the correspondence between optical target features and reflected image features. In this section, we describe a series of experiments investigating how distortion magnitude varies with image capture conditions.

In visits to operating heliostat fields, we noticed that reflected image distortion was extremely small when standing near a mirror and viewing objects in reflection but became much larger when inspecting sample metrology images. In some cases, the observed distortion exceeds what we felt could be addressed using automated image processing. We also noticed that the distances, both between the optical target and the mirror and the distance between the camera and the mirror, seemed to have an effect.

We conducted two experiments to systematically study this effect. We conducted these at the Sandia National Laboratories National Solar Thermal Test Facility (NSTTF). The NSTTF heliostat solar field layout is shown in Figure 2. These heliostats are used on a frequent basis and are known to provide good performance. Thus, the mirror quality and spacing between mirrors and the tower are exemplary of a practical, well-functioning solar field.

Our first experiment studied distortion for moderate target-to-mirror and camera-to-mirror distances. Figure 2 shows the setup. Using the last row of heliostats at NSTTF, we positioned the eastern heliostat 14E6 to face west. We then positioned all other heliostats to face south, except for one, which we also faced west (14E1 shown in Figure 2). This created a clear optical path between the mirror (14E6) and the optical target (the back side of 14E1). In the example shown in Figure 2, the target-to-mirror distance is 50 m. We then used a Nikon DSLR camera to capture images from positions with varying distance from the mirror. We used interchangeable zoom lenses and adjusted focal length to achieve similar pixel resolution across images. Figure 3 shows an example image, and the magenta square shows the portion of the image we cropped to provide a sample tile. Other than cropping and occasional slight rotation to compensate for camera tilt, no other image processing was performed.

The series of camera positions shown in Figure 2 provide a series of camera-to-mirror samples for the given heliostat-to-mirror distance for the selected target heliostat 14E1. We then moved 14E1 to face south and selected other heliostats to serve as optical targets. The resulting ensemble of experimental trials is illustrated in Figure 3. By selecting heliostats 14E4, 14E3, 14E1, 14W2, and 14W6 to serve as optical targets, we created target-to-mirror distances of 20 m, 30 m, 50 m, 70 m, and 110 m, respectively. For each of these, we captured images from positions with camera-to-mirror distances of 10 m, 20 m, 30 m, 50 m, 70 m, 90 m, and 110 m. This produced a two-dimensional exploration of the target-to-mirror and camera-to-mirror parameter space.

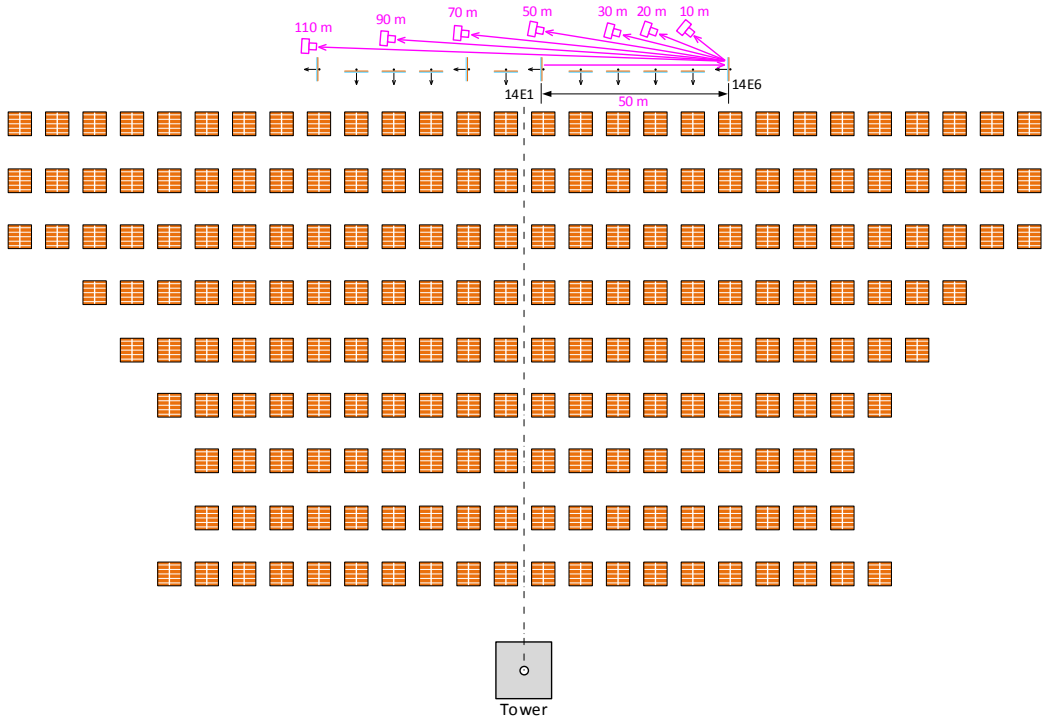

FIGURE 2. Using a row of heliostats to vary camera-to-mirror and heliostat-to-mirror distance.

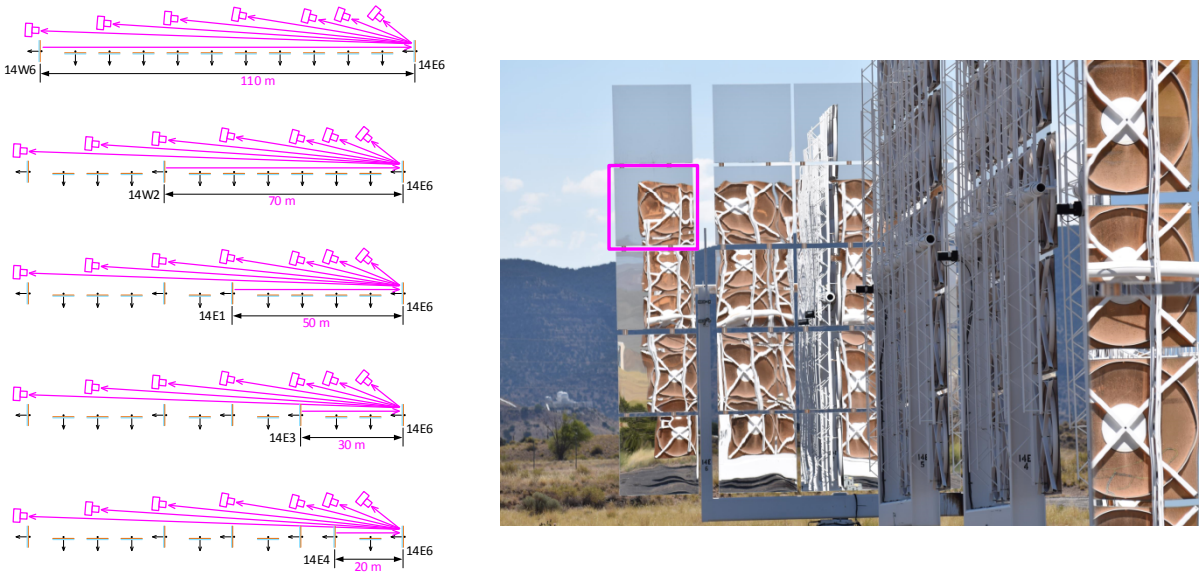

FIGURE 3. Left: Measurement scenarios. Right: Selecting a facet image.

After cropping the image as shown in Figure 3, we assembled the resulting image sample tiles into a matrix, shown in Figure 4. All image tiles show a reflection seen in heliostat 14E6; the selected facet varies slightly due to view angles. Examining this matrix of images shows a distinct increase in distortion with both heliostat-to-mirror and camera-to-mirror distance, with the most severe distortions occurring when both distances are high. The stark difference between the lower left and upper right tiles confirms that these parameters strongly influence distortion.

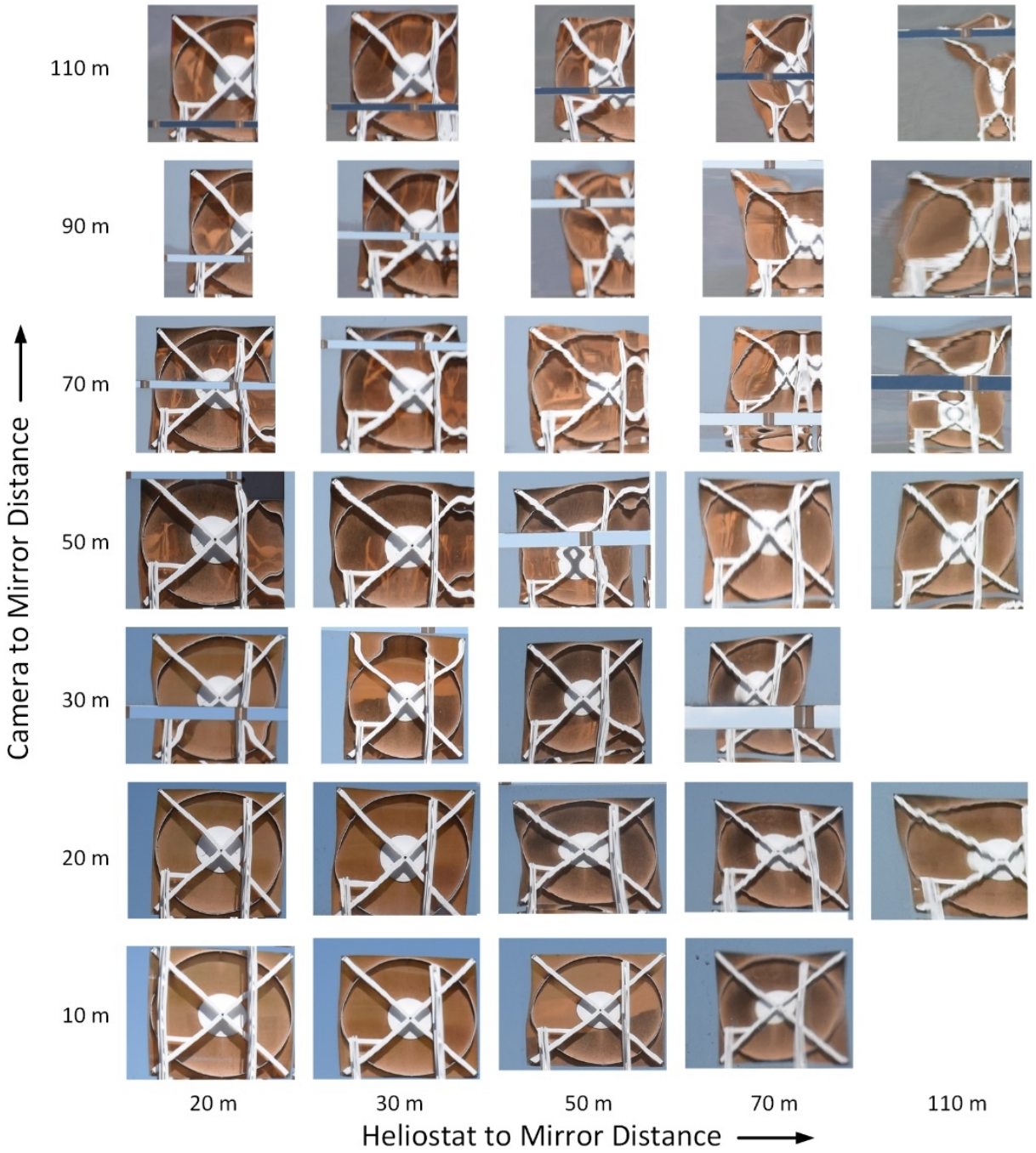

FIGURE 4. Heliostat facet reflections observed at different distances.

In the experiment shown in Figures 2-4, the maximum target-to-mirror distance is 110 m. But in some situations, the target-to-mirror distance may be much higher. For example, if the tower is used as an optical target [3], then the target-to-mirror distance may be as high as 1600 m for a large commercial solar field. To study this scenario, we conducted a second experiment designed to study much higher target-to-mirror distance.

Figure 5 shows the setup, using the NSTTF tower as the optical target. For target-to-mirror distances of 100 m and 190m, we were able to use NSTTF heliostats. However, more distant heliostats were not available on the NSTTF field. Thus we selected a planar NSTTF heliostat, mounted it on a fork lift, and positioned it at distances of 400 m, 800 m, 1200 m, and 1600 m from the tower. For each case, we captured images at camera-to-mirror distances of 25 m, 50 m, 100 m, and 150 m and cropped the image as shown in Figure 5.

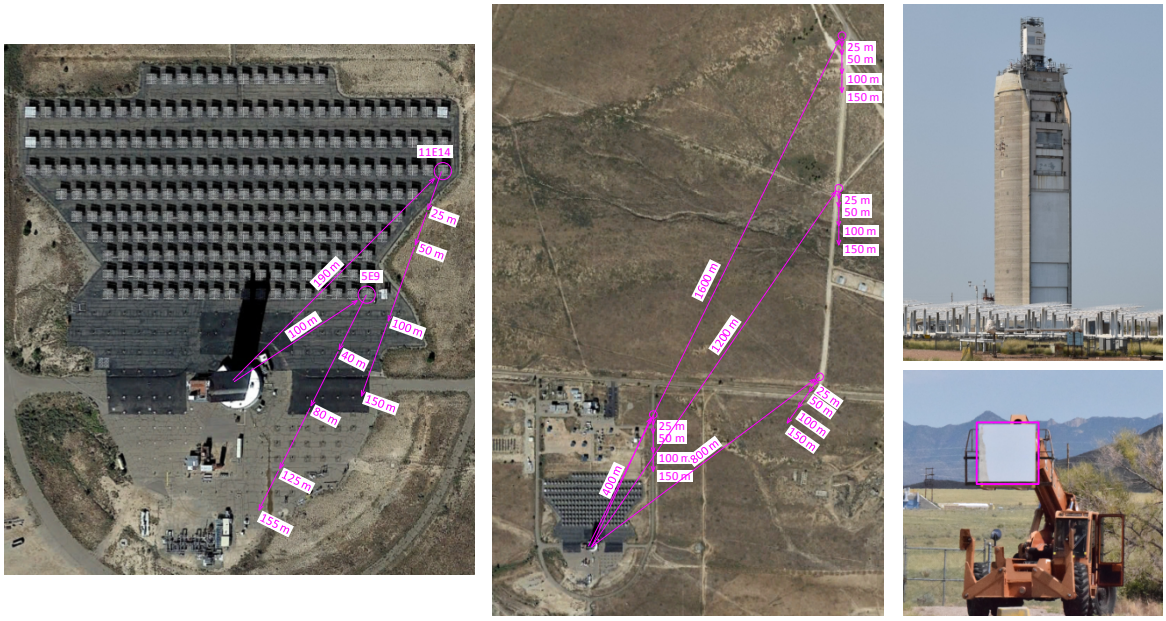

FIGURE 5. Left, Center: Long-range measurement scenarios. Right: Selecting a facet image.

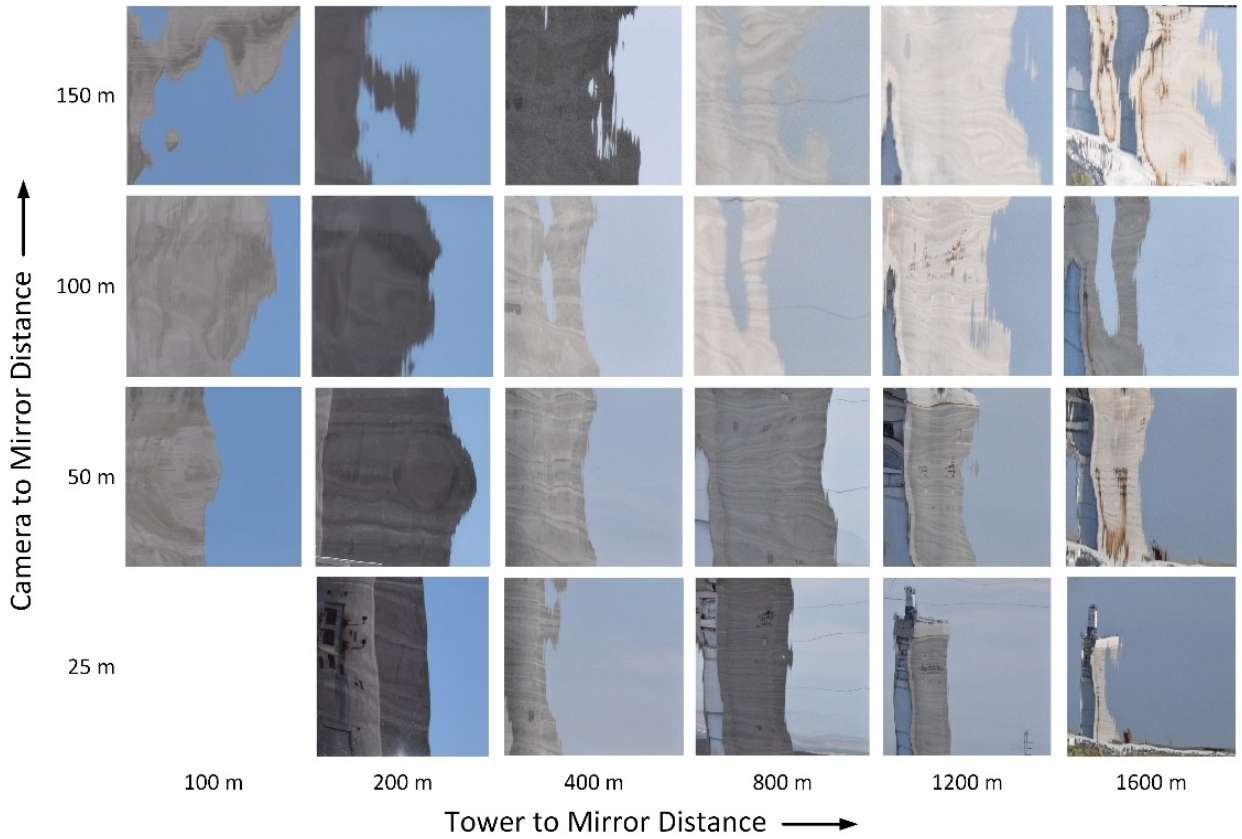

FIGURE 6. Reflection of the tower by a mirror facet at different distances.

Figure 6 summarizes the results. Again, we see distortion increasing with both tower-to-mirror and camera-to-mirror distance. In many cases, the observed distortion is so severe that the tower features are completely unrecognizable. Based on the results of the first experiment, this was expected. But if the camera-to-mirror distance is small (e.g., 25 m), then the growth in distortion with tower-to-mirror distance is not nearly so severe. Why?

MATHEMATICAL MODEL

To better understand distortion and how it depends on target-to-mirror and camera-to-mirror distance, we derived a mathematical model. Figure 7 shows defining parameters. We consider a camera C viewing a reflection of an optical target T in a mirror. Point R is the expected point of reflection, given in ideal mirror P_m. Without loss of generality, we place our coordinate system so the xy-plane contains the incident and reflected rays, with the coordinate system origin at point R. For an ideal mirror the reflection would be $T \rightarrow R \rightarrow C$. However, due to mirror shape and slope error, the actual mirror has a different local slope, indicated by the tilted plane P'_m with a local surface normal $\vec{n}'$ rotated an error angle ϵ from the ideal surface normal $\vec{n}$. Due to this slope, the reflection point is displaced to R'. The difference between R and R' is distortion, and we indicate the magnitude of this distortion by y_R. Distances d_T and d_C are the distances from the target and camera to the mirror, respectively.

In both the ideal and real mirror situations, Snell's Law of Reflection stipulates that the incident and reflected angles must be equal: $\theta_i = \theta_r$. Page limits do not allow us to present the full derivation, but the general approach is to transform the coordinates into the coordinates of the real mirror, cast the reflection problem as the solution of two simultaneous linear equations, and apply trigonometric identities. This derivation produces the following:

$$y_R = \frac{-2d_T d_C \cos(\epsilon)\sin(\epsilon)}{d_T \cos(\theta_i - \epsilon) + d_C \cos(\theta_i + \epsilon)} \#(1)$$

We implemented Equation (1) in a computer program and verified that it produces correct results across a range of situations.

We can improve our understanding by considering that slope error ϵ is typically a small angle, and for small ϵ angles $\theta_i \gg \epsilon$, $\cos(\epsilon) \approx 1$, and $\sin(\epsilon) \approx \epsilon$. Under this small angle assumption, Equation (1) simplifies to:

$$y_R = \frac{-2d_T d_C \epsilon}{\cos(\theta_i)[d_T + d_C]} \#(2)$$

This is our main result – an equation expressing distortion magnitude as a function of target-to-mirror distance d_T, camera-to-mirror distance d_C, and view incidence angle θ_i. We also implemented a computer verification of the small-angle assumption. We assumed a slope error $\epsilon = 10$ mrad and computed the discrepancy between the small angle model (2) and the full model (1). In two examples studied, the resulting discrepancies in y_R were 0.004% and 0.0002%, calculated with respect to smaller of d_T or d_C.

We can make several observations about this model:

- ✓ The sign of the error is correct for our example.
- ✓ Distortion grows linearly with slope error ϵ. (Within the small angle assumption.)
- ✓ As the incidence angle θ_i becomes very high, distortion grows rapidly (experiments not presented here).
- ✓ Distortion grows with both target-to-mirror and camera-to-mirror distance.
- ✓ Distortion grows rapidly (with the square) of the total optical path length.
- ✓ Both target-to-mirror and camera-to-mirror distance have a symmetric effect on distortion, if both are similar magnitude.

These match our observations. We can also consider the case for long-distance views, such as the tower reflections shown in Figure 6. In these circumstances $d_T \gg d_C$ and $d_T + d_C \approx d_T$. This allows us to simplify Equation (2):

$$y_R = \frac{-2d_C \epsilon}{\cos(\theta_i)} \#(3)$$

Thus, for long-range optical targets where $d_T \gg d_C$ we can make the following additional observation:

- ✓ Model matches long-distance tower-to-mirror observations, where distortion grew primarily with d_C.

This model therefore explains our observations shown in Figures 4 and 6:

1. For moderate distance reflections, distortion grows with both target-to-mirror and camera-to-mirror distance.
2. For long distance reflections, distortion grows primarily with camera-to-mirror distance.

Figure 8 shows a plot of Equation (3) for various combinations of d_T and d_C. It also shows a plot of a previous closely related model independently produced by Rebecca Mitchell and Guangdong Zhu at NREL [5].

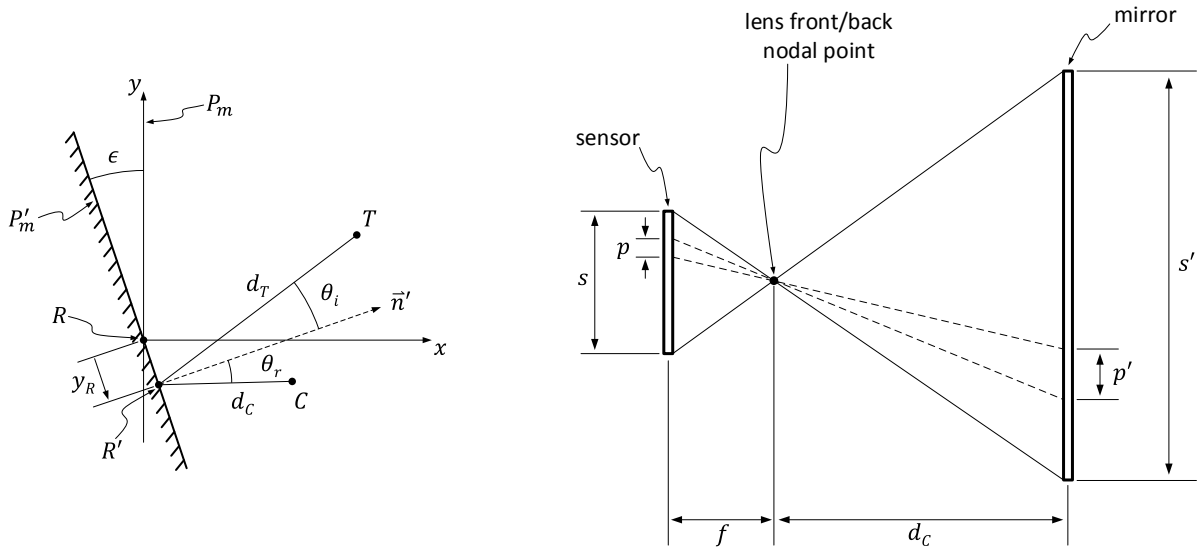

FIGURE 7. Left: Distortion model parameters. Right: Sensitivity model parameters.

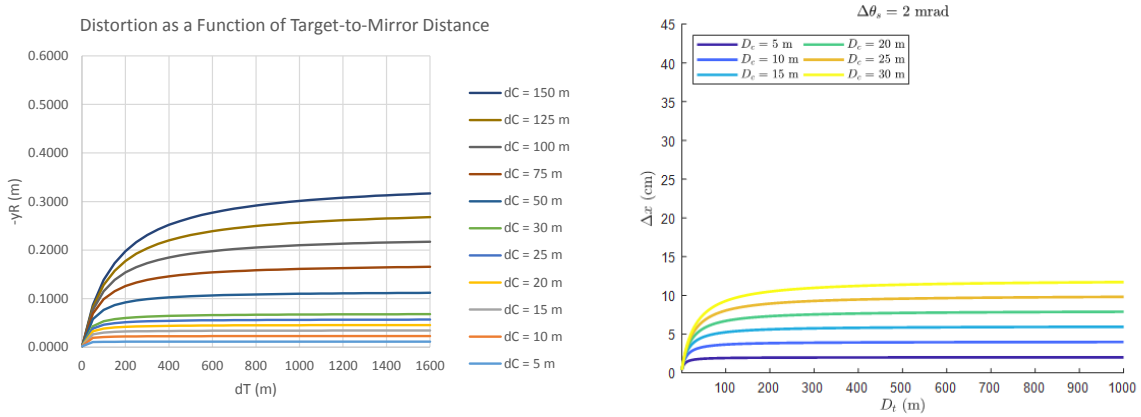

FIGURE 8. Left: Plot of the distortion model presented here. Right: A related NREL model [5].

METROLOGY SENSITIVITY

If we understand why distortion occurs and its driving parameters, then we can design our metrology systems to control it. Page limits prevent a full treatment of this topic, but here we will present a brief derivation of a sensitivity equation to aid metrology system design. Relevant parameters are shown in Figure 7.

First, we divide Equation (3) by the slope error ϵ:

$$\delta = \frac{2d_T d_C}{\cos(\theta_i)[d_T + d_C]} \#(4)$$

The parameter δ describes the sensitivity of the distortion displacement per unit slope error. It has units m/rad.

Next, we define a normalized camera focal length $F = f/s$, expressing the camera's focal length relative to the size of the image sensor. (A simple pinhole camera model is sufficient for our purposes here.) F is dimensionless. We also define $p' = d_C/nF$, where n is the number of sensor pixels along s. p' is the size of a sensor pixel projected onto the mirror surface, and has units m/pixel. Next, we invert this to form the pixel density at the mirror $\rho' = nF/d_C$, with units of pixels/m.

We then multiply Equation (4) by ρ':

$$n_\epsilon = \frac{2 d_T n F}{\cos\theta_i (d_T + d_C)} \#(5)$$

n_ϵ has units of pixel/rad and is the number of pixels displacement per unit slope error. It captures the sensitivity of a metrology system using design image capture conditions d_T, d_C, θ_i, n, and F. Since we can choose these parameters as part of our design, Equation (5) gives us a tool for understanding how various design decisions affect sensitivity, and for designing the system to achieve a desired sensitivity.

DISCUSSION

We have performed experiments with real CSP mirrors at realistic CSP scales and found that reflected image distortion can easily reach gross levels that make automated feature recognition in image processing exceedingly difficult, if not impossible. However, we have also seen that selecting appropriate target-to-mirror and camera-to-mirror distances can greatly reduce observed distortion. This understanding enables selection of image capture parameters to achieve metrology goals.

Another type of distortion, not discussed here due to page limits, results from the optical focus of a concave mirror. For example, a parabolic mirror of focal length f, viewed from an observation points on the optical axis and distance $d_C = 2f$ results in an optical collapse where image features are completely scrambled. This effect provides an opportunity for another type of mirror metrology, explained in [6].

We note that other metrology approaches such as deflectometry [7,8]) do not require a coherent image, and thus are not vulnerable to distortion effects. However, deflectometry requires a large projector screen, a static scene, illumination control (if fringe based), and clean mirrors, all difficult outdoors.

ACKNOWLEDGMENTS

We thank Roger Buck, Robert Crandell, and Luis Garcia Maldonado for their assistance with the distortion measurements. We also thank the DOE Solar Energy Technologies Office for their support. Sandia National Laboratories is a multimission laboratory managed and operated by National Technology & Engineering Solutions of Sandia, LLC, a wholly owned subsidiary of Honeywell International Inc., for the U.S. Department of Energy's National Nuclear Security Administration under contract DE-NA0003525.

REFERENCES

[1] E. Sproul, K. Chavez, and J. Yellowhair, "The Development of the Heliostat Focusing and Canting Enhancement Technique: An Optical Heliostat Alignment Tool for the National Solar Thermal Test Facility." *Proceedings of the 2011 International Conference on Energy Sustainability and Fuel Cell Science, Engineering, and Technology Conference (ESFuelCell2011).* Washington, DC, Aug. 2011.

[2] J. Yellowhair, P. Apostolopoulos, D. Small, D. Novick, and M. Mann. "Development of an Aerial Imaging System for Heliostat Canting Assessments," presented in *2020 SolarPACES.*

[3] R. Mitchell and G. Zhu, "A Non-Intrusive Optical (NIO) Approach to Characterize Heliostats in Utility-Scale Power Tower Plants: Methodology and in-situ Validation." *Solar Energy* **209**, pp. 431-445, 2020.

[4] R. Brost, P. Apostolopoulos, D. Small, D. Novick, N. Jackson, M. Mann, and E. Tsiropoulou. "High-Speed In Situ Optical Scanning of Heliostat Fields," presented in *2021 SolarPACES.*

[5] R. Mitchell and G. Zhu. "A non-intrusive optical (NIO) approach to characterize heliostats in utility-scale power tower plants: Sensitivity study." *Solar Energy* **207**, 2020.

[6] J. Strachan, *Revisiting BCS, a Measurement System for Characterizing the Optics of Solar Collectors*. Albuquerque, NM: Sandia National Laboratories, SAND92-2789C, 1992.

[7] C. Andraka, S. Sadlon, B. Myerr, K. Trapeznikov, and C. Liebner. "Rapid Reflective Facet Characterization Using Fringe Reflection Techniques." *Journal of Solar Energy Engineering* **136**, Feb. 2014.

[8] S. Ulmer, T. Marz, C. Prahl, W. Reinalter, B. Belhomme. "Automated high resolution measurement of heliostat slope errors." *Solar Energy* **85**, 2011.